Dependence of Fracture Toughness of Austempered Ductile Iron on Austempering Temperature

P. PRASAD RAO and SUSIL K. PUTATUNDA

Ductile cast iron samples were austenitized at 927 °C and subsequently austempered for 30 minutes, 1 hour, and 2 hours at 260 °C, 288 °C, 316 °C, 343 °C, 371 °C, and 399 °C. These were subjected to a plane strain fracture toughness test. Fracture toughness was found to initially increase with austempering temperature, reach a maximum, and then decrease with further rise in temperature. The results of the fracture toughness study and fractographic examination were correlated with microstructural features such as bainite morphology, the volume fraction of retained austenite, and its carbon content. It was found that fracture toughness was maximized when the microstructure consisted of lower bainite with about 30 vol pct retained austenite containing more than 1.8 wt pct carbon. A theoretical model was developed, which could explain the observed variation in fracture toughness with austempering temperature in terms of microstructural features such as the width of the ferrite blades and retained austenite content. A plot of K_{IC}^2 against $\sigma_y (X_\gamma C_\gamma)^{1/2}$ resulted in a straight line, as predicted by the model.

I. INTRODUCTION

WHEN ductile iron is subjected to an austempering treatment, a range of microstructures is obtained depending on heat treatment parameters such as austenitizing time and temperature and austempering time and temperature.[1–5] This results in austempered ductile irons (ADIs) of different grades ranging from high-strength–low-ductility types, to low-strength–high-ductility ones, which have been found to be economical substitutes for high strength steels in several applications. The influence of heat treatment parameters on the microstructure has been extensively studied using optical microscopy, electron microscopy, and X-ray diffraction. It is now understood that the austempering reaction in ductile iron is a two-stage process. At the austempering temperature, ferrite precipitates out of, and grows into, the austenite. Simultaneously, carbon is rejected from the growing ferrite plates into the surrounding austenite. Carbide precipitation is suppressed because of the high silicon content. The enrichment of austenite with carbon inhibits the growth of ferrite and also stabilizes the austenite. This decomposition of austenite into ferrite and high carbon austenite is referred to as the stage I reaction. If now quenched from the austempering temperature, the microstructure will consist of ferrite platelets in a matrix of stabilized high carbon austenite. This is the desired microstructure of ADI. If the iron is held at the austempering temperature for too long a time, the high carbon austenite will decompose into ferrite and carbide. This is the stage II reaction and is not desired, as the carbide precipitation will embrittle the iron. If the austempering time is too short, the austenite may not be fully enriched with carbon, and some of it may transform to martensite on quenching, again leading to embrittlement of the iron. The optimum austempering time is, therefore, the period between the end of stage I and the beginning of stage II. This is called the processing window.

The influence of microstructure on mechanical properties such as hardness, yield strength, tensile strength, and ductility has been reported by several investigators.[10–11] The important microstructural features of ADI that influence their mechanical properties are retained austenite content, carbon content of retained austenite, morphology of ferrite, precipitated carbide if any, and the presence of any unstabilized austenite that transformed to martensite. The number of graphite patches, their size, distribution, and nodularity are also important factors. However, these are unaffected by heat treatment conditions and are influenced only by melting and casting practice. Therefore, while studying the influence of heat treatment parameters on mechanical properties, these are generally ignored.

Fracture toughness is an important mechanical property. An understanding of the influence of microstructure on fracture toughness is important in order to optimize heat treatment parameters. Previous investigations have shown the importance of austempering temperature in controlling fracture toughness.[12–15] These studies have shown that ADI with lower bainitic microstructure has better fracture toughness than that with upper bainitic microstructure. It has also been shown that a retained austenite content of around 25 vol pct is desirable and that increasing the carbon content of the austenite increased fracture toughness. The present investigation has been undertaken to study further the influence of microstructure on fracture toughness and to develop a model relating fracture toughness and microstructural features such as the retained austenite content, the carbon content of retained austenite, and the width of the ferrite blade.

II. EXPERIMENTAL WORK

The chemical composition of the ductile iron used in the present investigation is shown in Table I. Compact tension

P. PRASAD RAO, Professor, is with the Department of Metallurgical and Materials Engineering, Karnatak Regional Engineering College, Karnatak State, India 574 157. SUSIL K. PUTATUNDA, Associate Professor, is with the Department of Chemical Engineering and Materials Science, College of Engineering, Wayne State University, Detroit, MI 48202.

Manuscript submitted January 14, 1998.

Table I. Chemical Composition of the Ductile Iron (in Weight Percent)

C	3.54
Si	2.81
Mn	0.43
S	0.009
P	0.031
Mg	0.05
Ni	1.52
Mo	0.30
Cu	0.56
Cr	0.30

specimens machined from cast slabs were austenitised at 927 °C for 2 hours. These were then austempered at 260 °C, 288 °C, 316 °C, 343 °C, 371 °C, and 399 °C for 30 minutes, 1 hour, and 2 hours. Fracture toughness testing was carried out per ASTM-E399 on an MTS 810 servohydraulic machine. Fracture surfaces of the fracture toughness samples were examined on a Hitachi S-2400 scanning electron microscope. Samples were cut from the fracture toughness specimens for optical metallography and X-ray diffraction. The volume fraction of retained austenite and its carbon content were estimated by the X-ray diffraction technique. The complete experimental procedure is explained elsewhere.[15]

III. RESULTS AND DISCUSSION

Fracture toughness results are presented in Figure 1, which shows the variation of fracture toughness with austempering temperature at the three austempering times employed in the present investigation. As the austempering temperature is increased, the fracture toughness initially rises, reaches a peak, and then decreases with further increase in temperature. This trend is similar to that observed by other investigators.[12–17] The same behavior is observed at all three austempering times. The fracture toughness increases with increasing austempering time. However, beyond 316 °C, the difference between samples austempered for 1 and 2 hours is rather small. There is a perceptible shift in the peak to higher temperatures, with decreasing austempering time.

Fracture surfaces were examined under the scanning electron microscope to elicit information on fracture mechanism. Samples austempered for 2 hours exhibited either fully dimpled ductile fracture or dimpled fracture in association with a varying degree of transgranular cleavage fracture. Those austempered at 288 °C and 316 °C showed completely ductile fracture, while others showed some presence of cleavage fracture, as shown in Figure 2. Samples austempered for 30 minutes showed either intergranular or transgranular type of fracture. Those austempered for 1 hour showed all the types mentioned above, depending on the temperature. Figures 3 and 4 show fractographs of samples austempered for 30 minutes and 1 hour, respectively, at 260 °C, 316 °C, and 399 °C. Figure 5 summarizes the results of fractographic examination. Lines are drawn to highlight regions of predominantly the same type of fracture on this time-temperature map. Fracture toughness values are also shown. While samples austempered for 1 hour at 316 °C and for 2 hours at 288 °C and 316 °C showed

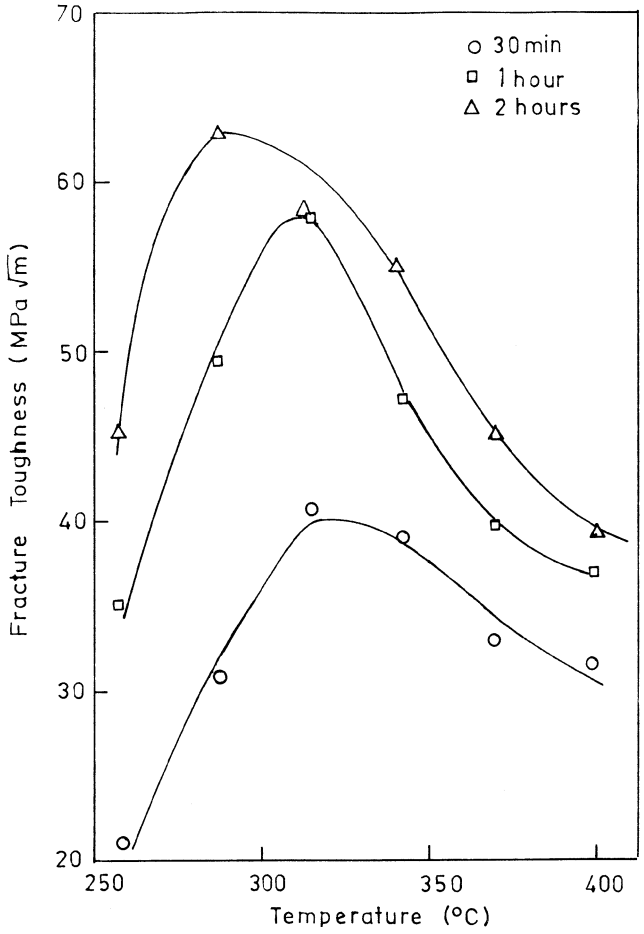

Fig. 1—Influence of austempering temperature on fracture toughness at different austempering times.

fully ductile fracture, all others showed a varying degree of cleavage fracture, bringing out the strong influence of microstructure on fracture toughness.

Figure 6 shows the microstructures of the samples austempered for 2 hours at each of the temperatures. Samples austempered at 316 °C and below showed the typical lower bainitic microstructure, while those austempered at higher temperatures exhibited typical upper bainitic microstructures. When austempered for shorter times, untransformed austenite was observed, the amount increasing with decreasing temperature at a given austempering time. This is shown by typical micrographs in Figures 7 and 8, of samples austempered for 30 minutes and 1 hour at 288 °C and 343 °C, respectively. Samples that exhibited the best fracture toughness had lower bainitic microstructure consisting of fine laths of ferrite.

Retained austenite content and carbon content of retained austenite were estimated by X-ray diffraction technique. The samples were scanned in the angular 2θ range of 42 to 46 deg and 70 to 105 deg to obtain the (110) and (211) peaks of ferrite and the (111), (220), and (311) peaks of austenite. The profiles were processed in a computer to obtain the peak positions as well as the integrated intensities of the peaks. The volume fraction of the retained austenite was then determined by the direct comparison method. Repeated scans of the same samples, as well as scans at mutually perpendicular orientations of a given sample, showed

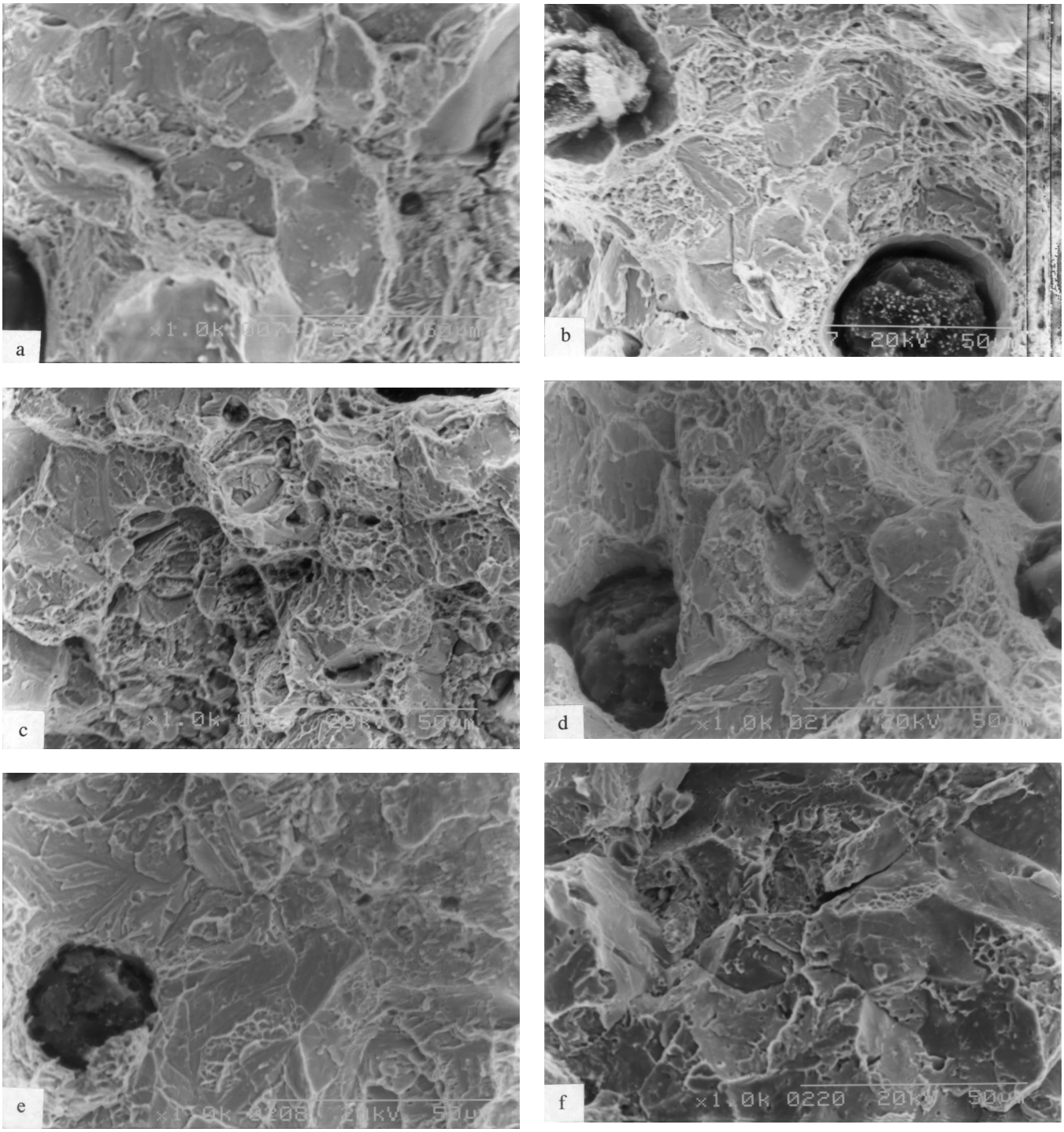

Fig. 2—Fractographs of samples austempered for 2 h at (*a*) 260 °C, (*b*) 288 °C, (*c*) 316 °C, (*d*) 343 °C, (*e*) 371 °C, and (*f*) 399 °C.

that there was no appreciable scatter and that the results were accurate within ± 5 pct. Figure 9 shows the influence of austempering temperature on retained austenite content at different times. It shows that the retained austenite content increases with increasing austempering temperature. At all temperatures, a large increase in retained austenite content is observed from 30 minutes to 1 hour. However, the variation in austenite content with a further increase in time is sensitive to temperature. This increase decreases with temperature from 260 °C to 316 °C, and was in the range of 40 to 10 pct, while at the higher temperatures, the difference was practically negligible, being in the range of ± 3 pct. It may be concluded that samples austempered for 1 hour at temperatures 316 °C and higher are within the processing window. Figure 10 is a plot of retained austenite content against austempering time at different temperatures. Superimposed on this are curves indicating the different fracture mechanisms observed, which helps in correlating the fracture mechanisms with austenite contents. Fully ductile fracture was observed in samples that had austenite content of around 30 vol pct. These had the highest fracture toughness.

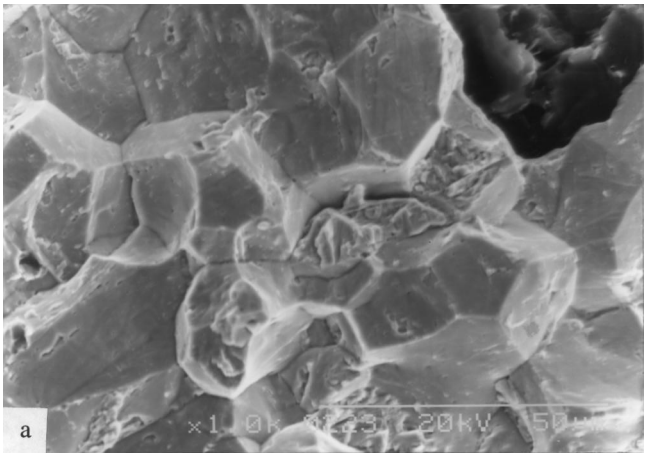

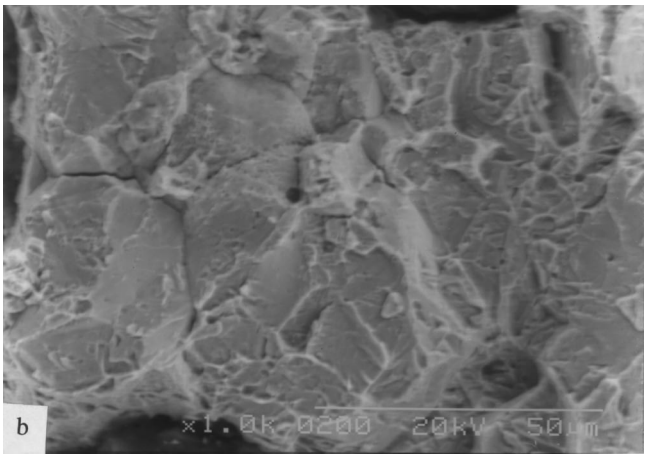

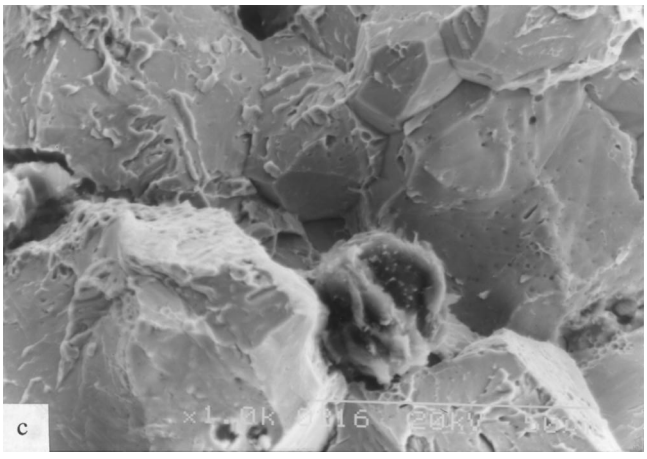

Fig. 3—Fractographs of samples austempered for 30 min at (*a*) 260 °C, (*b*) 316 °C, and (*c*) 399 °C.

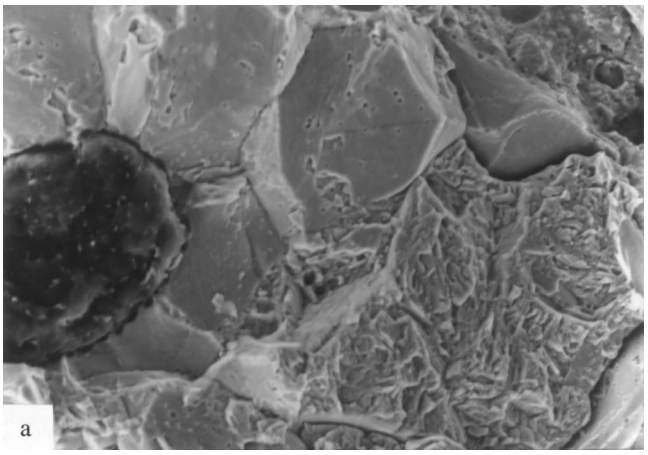

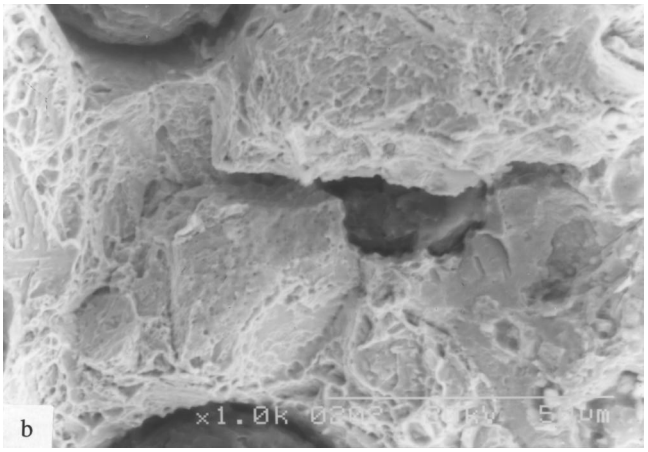

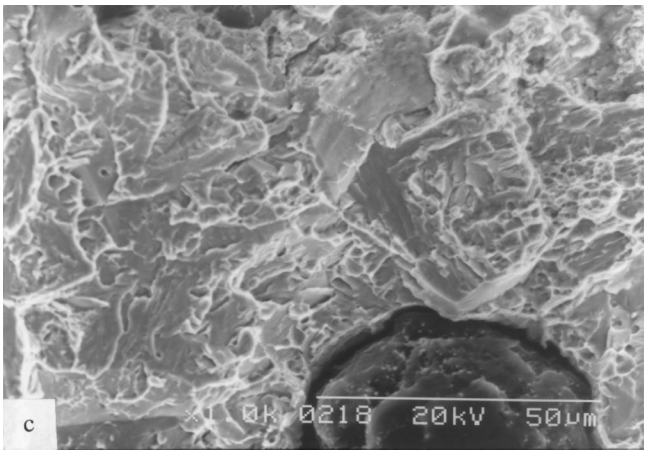

Fig. 4—Fractographs of samples austempered for 1 h at (*a*) 260 °C, (*b*) 316 °C, and (*c*) 399 °C.

Figure 11 shows the dependence of carbon content of retained austenite on temperature at different times. Carbon content rises with temperature until 316 °C and decreases beyond that. Considering Hultgren's extrapolation of the ferrite + austenite region of the iron-carbon phase diagram to temperatures below the eutectoid as valid in the present case, one should expect decreasing carbon content in austenite with increasing temperature. But this is not observed at temperatures lower than 316 °C. This should be attributed to slow diffusion at low temperatures. At such low diffusion rates, 2 hours are not sufficient to build up the carbon content in the austenite. Curves are superimposed on this diagram to indicate fracture mechanisms associated with different carbon levels. When carbon content is more than 1.8 wt pct, there is a high probability of ductile fracture.

Figure 12 shows the combined effect of retained austenite content and its carbon content. The best fracture toughness is obtained when retained austenite content is about 30 vol pct and its carbon content is more than 1.8 wt pct. Therefore, microstructurally, the following features are necessary to obtain optimum fracture toughness in ADI:

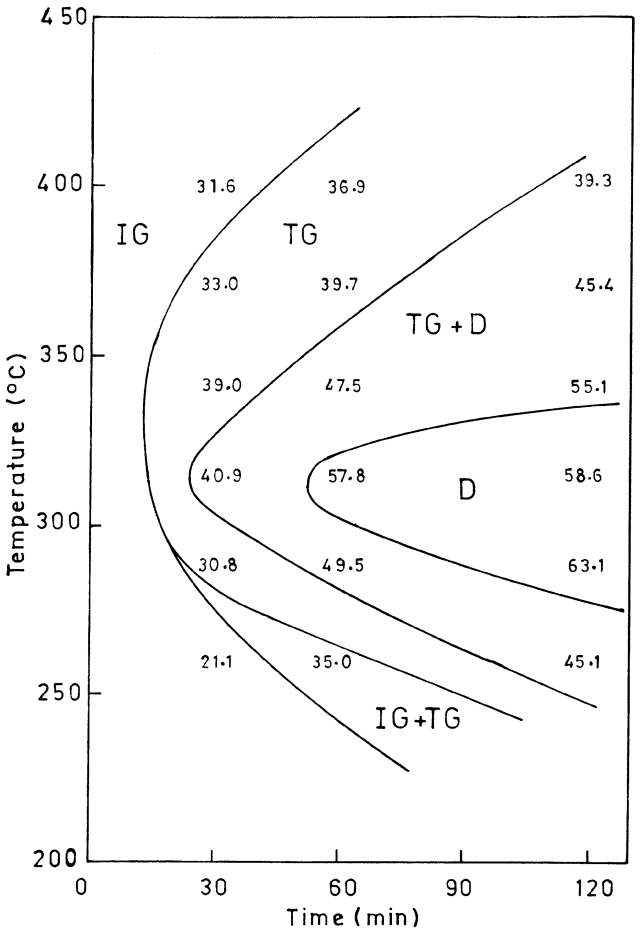

Fig. 5—Fracture mechanism under different austempering conditions. D: ductile, TG: transgranular cleavage, and IG: intergranular cleavage.

(a) lower bainitic microstructure consisting of fine ferrite laths;
(b) retained austenite content of around 30 vol pct; and
(c) a high carbon content of the retained austenite of more than 1.8 wt pct.

The fracture toughness should reach some maximum value when plotted as a function of austempering temperature due to the interplay between the effects of ferrite grain size and austenite volume fraction. Ferrite has a maximum toughness at the lowest austempering temperature because it then has the finest grain size. On the other hand, the austenite content increases with austempering temperature. The contribution to fracture toughness from austenite increases with increasing temperature. Actual toughness would be controlled by the weakest link, which is austenite at low temperatures and ferrite at high temperatures.

Let us first look at the effect of austenite content. It has been reported[18,19] that crack initiation in ADI starts with decohesion of the weak graphite/matrix interface. This creates a stress concentration in the matrix around the graphite nodules. The ADI matrix consists of ferrite needles and high carbon austenite. The carbon content of the austenite is in the range of 1.6 to 2.0 wt pct, depending on the heat treatment condition. The high carbon austenite is a tough phase. It has a high strain hardening tendency. But the ferrite is a softer phase. It has been shown that plastic deformation in the matrix ahead of the regions of decohesion will be confined essentially to these isolated soft ferrite regions.[18] When cracks form within these due to severe plastic deformation, they remain isolated since the crack finds it difficult to move across the broad regions of tough austenite to join up with similar microcracks in the neighboring ferrite needles. Thus, crack propagation becomes difficult. Therefore, one can expect the fracture toughness to increase with the volume fraction of austenite. Since the volume fraction of austenite increases with the austempering temperature, on the basis of the preceding argument, the fracture toughness will also increase with the austempering temperature.

The toughness of the constituents depends on their ductility under applied load. The major portion of the crack extension force driving a crack is dissipated in extending the plastic zone. Since the energy required to deform a unit volume of the material is represented by the area under the stress-strain curve, the critical energy or work, W, to deform a unit volume of material to fracture may be computed by

$$W = \sigma_{ys}\varepsilon_f \qquad [1]$$

where W is the work of deformation to fracture (per unit volume), σ_{ys} is yield stress, and ε_f is true strain at fracture (plastic component). Within this unit volume, a fraction X_α is ferrite and X_γ is austenite. Hence, we can write

$$W = X_\alpha\sigma_{ys\alpha}\varepsilon_{f\alpha} + X_\gamma\sigma_{ys\gamma}\varepsilon_{f\gamma} \qquad [2]$$

The volume of deformed metal associated with the extension of a crack by dx is $(2V_c)\,Bdx$, where $2V_c$ is the crack opening displacement and B is the material thickness. We have

$$G = \frac{dW}{Bdx} \qquad [3]$$

Therefore,

$$G_{Ic} = 2V_c\sigma_{ys}\varepsilon_f \qquad [4]$$

Using Eq. [2], Eq. [4] can be written as

$$G_{Ic} = X_\alpha 2V_c\sigma_{ys\alpha}\varepsilon_{f\alpha} + X_\gamma 2V_c\sigma_{ys\gamma}\varepsilon_{f\gamma} \qquad [5]$$

Since

$$G = \frac{K^2}{E} \qquad [6]$$

we now have

$$K_{Ic} = \left[X_\alpha 2V_c\sigma_{ys\alpha}\varepsilon_{f\alpha} + X_\gamma 2V_c\sigma_{ys\gamma}\varepsilon_{f\gamma}\right]^{1/2} E^{1/2} \qquad [7]$$

Hahn and Rosenfield[20] have studied in detail the relation between fracture toughness, crack opening displacement, and other mechanical properties of a large number of alloy systems. Using their relationship, we arrive at the final form of the equation:

$$K_{Ic} = \left[0.017n_\alpha^2 X_\alpha\sigma_{ys\alpha}\varepsilon_{f\alpha} + 0.017n_\gamma^2 X_\gamma\sigma_{ys\gamma}\varepsilon_{f\gamma}\right]^{1/2} E^{1/2} \qquad [8]$$

where n_α and n_γ are strain hardening coefficients of α and γ, respectively. The dependence of fracture toughness on the volume fraction of austenite was estimated by incorporating the following typical values for various terms in

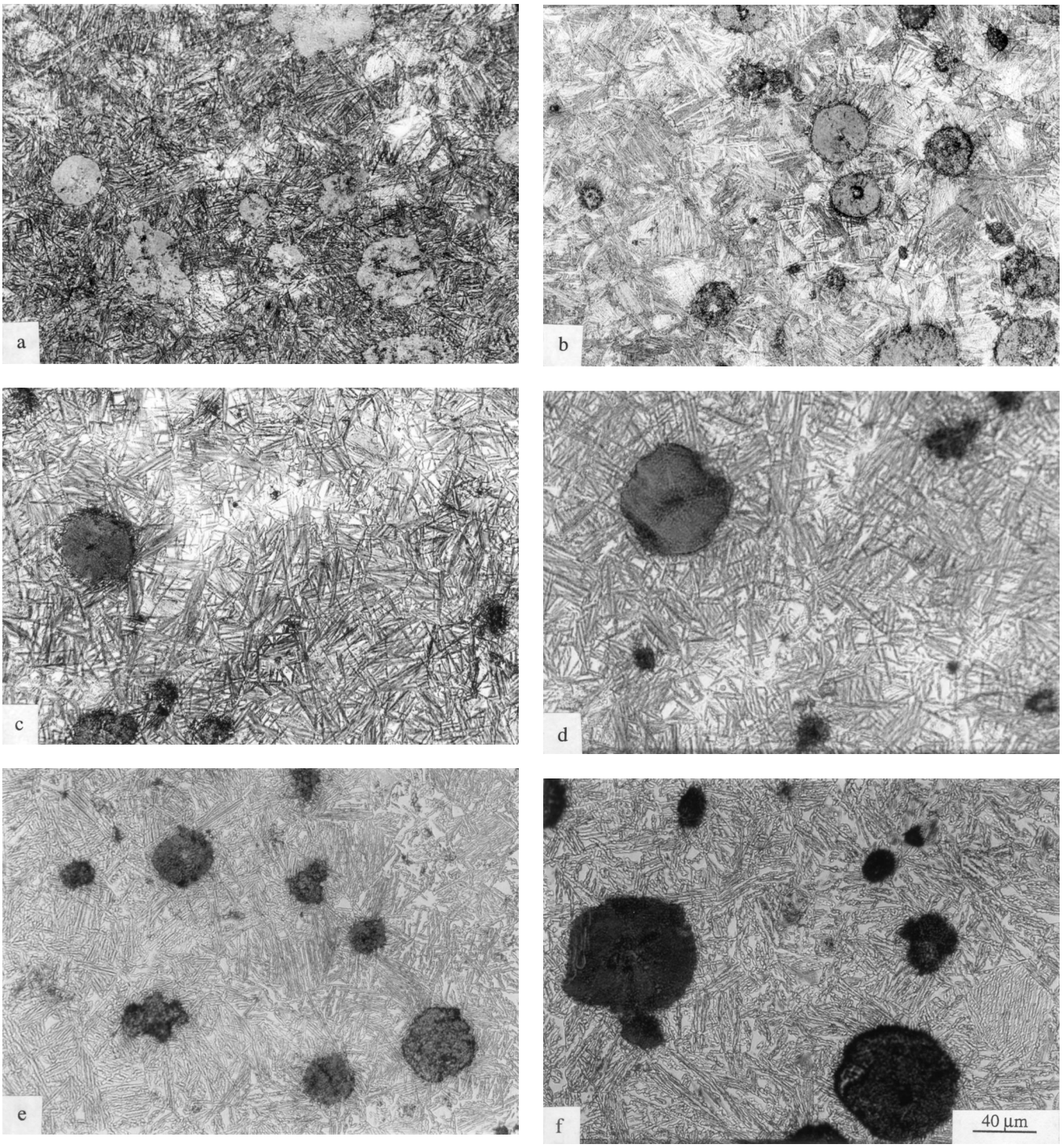

Fig. 6—Microstructures of samples austempered for 2 h at (*a*) 260 °C, (*b*) 288 °C, (*c*) 316 °C, (*d*) 343 °C, (*e*) 371 °C, and (*f*) 399 °C.

Eq. [8]: $\sigma_{s\alpha} = 200$ MPa, $\sigma_{s\gamma} = 400$ MPa, $\varepsilon_{f\alpha} = 0.2$, $\varepsilon_{f\gamma} = 0.3$, $n_\alpha = 0.1$, $n_\gamma = 0.4$, and $E = 2.7$ GPa. The variation of fracture toughness with the volume fraction of austenite is shown in Figure 13. The first term inside the bracket is small as compared to the second term. Therefore, the fracture toughness will be primarily determined by the austenite content. It can be seen that as the asutenite content increases, the fracture toughness increases.

Let us now consider the effect of ferrite width on fracture toughness. The plastic deformation that exists in the ADI matrix around the graphite nodules can be considered to be inhomogeneous in nature, as it is primarily confined to the softer ferrite phase. Such an inhomogeneous plastic deformation can lead to crack formation. Consider a glide band containing many moving dislocations, emitted from a source within the ferrite needle. Such a band can be treated as a viscous inclusion within an elastic matrix. It cannot support any shear stress. All of it must concentrate at its tip. If the band is now blocked by the ferrite/austenite interface, large tensile as well as shear stresses will be de-

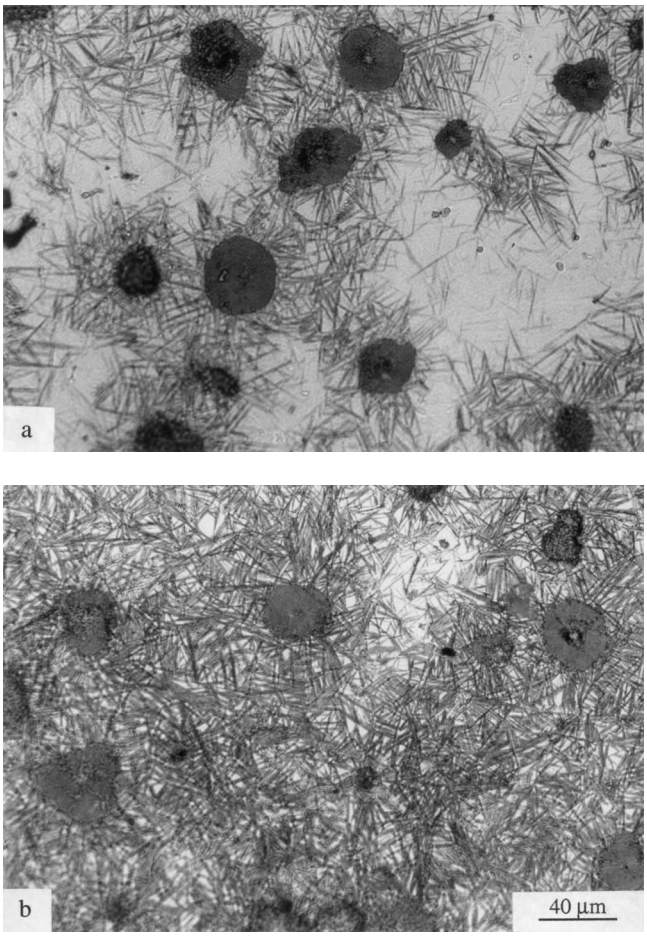

Fig. 7—Microstructures of samples austempered at 288 °C for (*a*) 30 min and (*b*) 1 h.

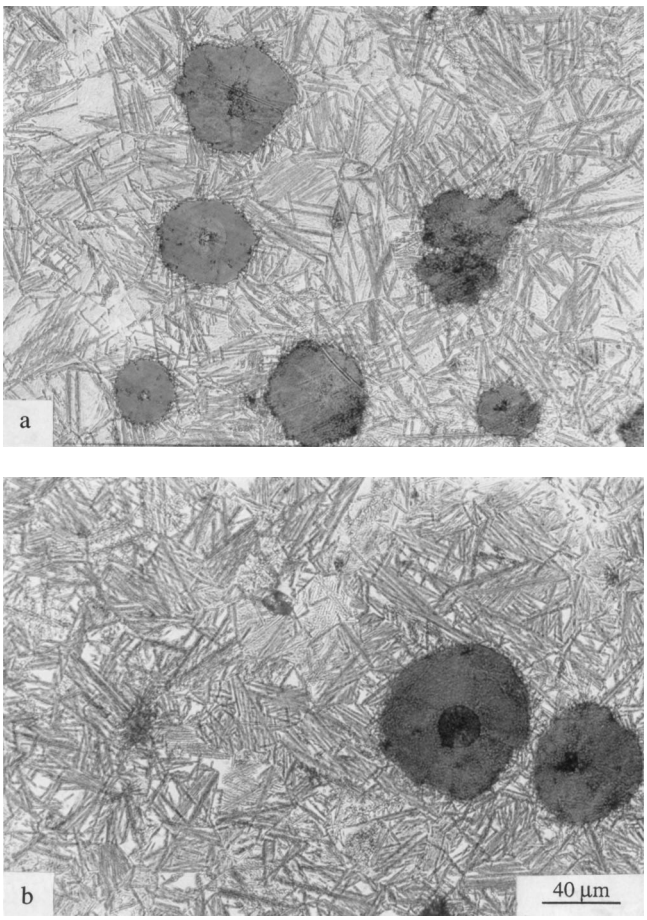

Fig. 8—Microstructures of samples austempered at 343 °C for (*a*) 30 min and (*b*) 1 h.

veloped at its tip. Consider a pileup of n dislocations to form a glide band of length $L/2$, where L is the width of the ferrite blade. All of the applied shear stress τ is relaxed inside the band, except for the friction stress τ_i, which opposes dislocation motion. The plastic displacement near the tip is given as nb, where b is the Burgers vector. We now have

$$n = \frac{L\,(\tau - \tau_i)}{2G\mathrm{b}} \qquad [9]$$

The concentrated tensile stress σ_L at some point (r, Φ) from the tip of the pileup is

$$\sigma_L = (\tau - \tau_i)\,(\frac{L}{2r})^{1/2}\,F(\phi) \qquad [10]$$

Crack initiation occurs when this concentrated tensile stress at the tip of the band is equal to the theoretical cohesive stress:

$$\sigma_c = \sqrt{\frac{E\gamma_s}{a_0}} \qquad [11]$$

where E is the Young's modulus, γ_s is the surface energy, and a_0 is the lattice parameter. Now from Eqs. [10] and [11],

$$(\tau - \tau_i)\,(\frac{L}{2r})^{1/2} \geq \sqrt{\frac{E\gamma_s}{a_0}} \qquad [12]$$

On the left-hand side of Eq. [12], the maximum value of Eq. [10] is taken. Therefore, shear stress for crack nucleation can be written as

$$\tau_N = \tau_i + \sqrt{\frac{Er\gamma_s}{(L/2)a_0}} \qquad [13]$$

We assume that $r = a_0$ and $E = 2G$.

Then

$$\tau_N = \tau_i + \sqrt{\frac{2G\gamma_s}{L/2}} \qquad [14]$$

Since crack initiation can occur simultaneously at a large number of sites due to the presence of many graphite nodules and fine ferrite/austenite spacing, these cracks once initiated can link up with the neighboring cracks and easily grow to the critical length. The fracture toughness can now be estimated. We have

$$K_{Ic} = \sigma\sqrt{\pi a} \qquad [15]$$

where a is the half-critical crack length. We now substitute σ with $2\tau_N$. Then

$$K_{Ic} = 2(\tau_i + \sqrt{\frac{2G\gamma_s}{L/2}}) \qquad \sqrt{\pi a} \qquad [16]$$

Here, L is the average width of the ferrite needles. We take the following values for the constants, from literature:

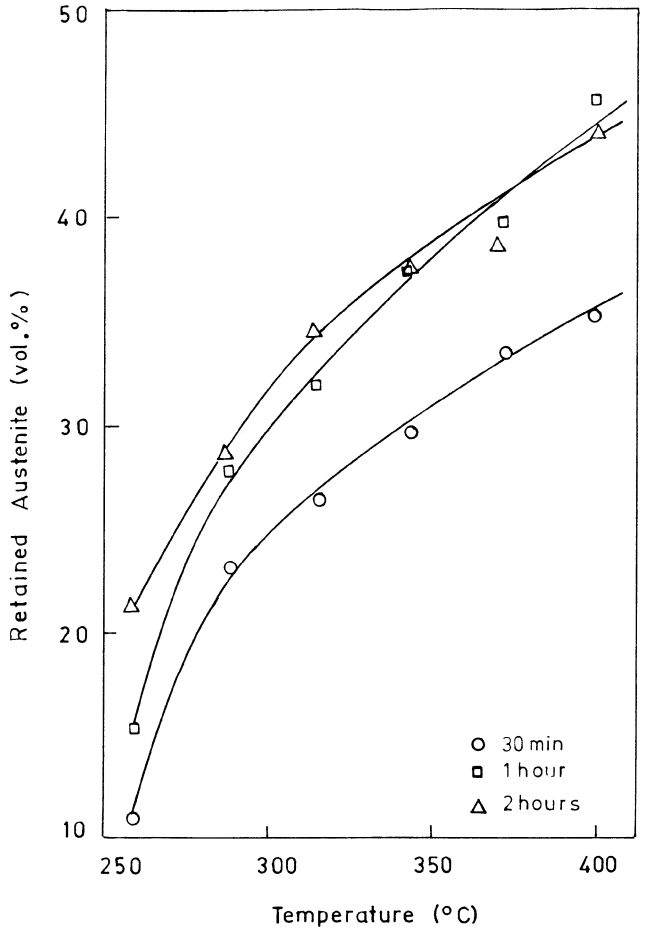

Fig. 9—Retained austenite content as a function of austempering time.

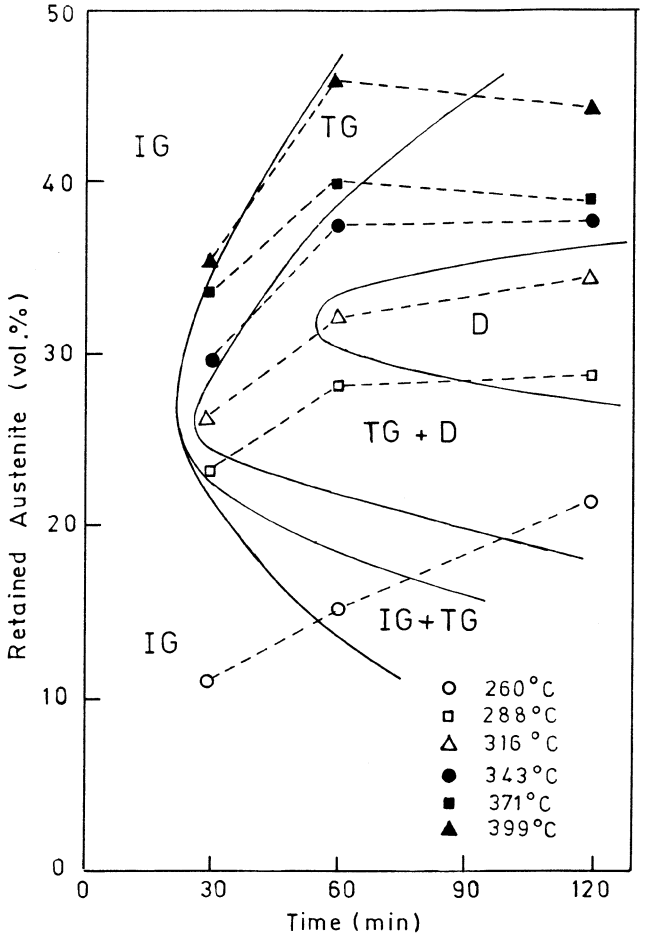

Fig. 10—Fracture mechanism at different austenite contents.

$$G = \frac{E}{2(1 + \nu)} = \frac{207}{2(1 + 0.3)} = 80.0 \text{ GPa}^{(22)}$$

$$\gamma_s = \text{surface energy} = 1.9 \text{ J m}^{-2}{}^{(23)}$$

The variation of fracture toughness with the width of the ferrite needles was calculated taking the critical crack length to be 2 mm, and the result is shown in Figure 14. It can be seen that fracture toughness rises with decreasing ferrite width. Since the ferrite needle becomes finer as the austempering temperature decreases, the model suggests that fracture toughness increases as the austempering temperature decreases.

The variation of actual fracture toughness depends on a combination of these two mechanisms. Since both ferrite width and volume fraction of austenite are dependent on austempering temperature, it is of interest to see the dependence of fracture toughness on austempering temperature. For this, one needs values of ferrite width and volume fraction of austenite at different austempering temperatures and corresponding values of fracture toughness. Austenite contents of samples austempered for 2 hours at different temperatures were used in calculating fracture toughness from Eq. [8]. Fracture toughness was then plotted against temperature and is shown as curve 1 in Figure 15. The width of the ferrite blades in ADI were measured from transmission electron micrographs available in literature[24,25,26] and were typically 0.15 μm at 300 °C, 0.6 μm at 350 °C, and 1.6 μm at 400 °C. It should be noted that these are from a very limited number of micrographs. But the work currently in progress in our laboratories indicates that these are good approximations. These values of ferrite width were used in calculating fracture toughness from Eq. [16] and were plotted as curve 2 in Figure 15. When the ferrite width is very small, the second mechanism requires high stresses. The fracture is then controlled by the first mechanism. At high widths of the ferrite blades, the second mechanism requires lower stress and will determine the fracture toughness of the material. The optimum fracture toughness is obtained at 300 °C at the intersection of the two curves. At low austempering temperatures, the fracture toughness follows curve 1 and changes over to curve 2 at higher temperatures. Such a resultant curve is shown as curve 3 in the figure. This curve rises with increasing austempering temperature, reaches a peak at 300 °C, and drops thereafter with a further rise in temperature. This matches well in a qualitative sense with the curve for samples austempered for 2 hours in Figure 1. If austempered for shorter durations, say 1 hour, curve 1 in Figure 15 will shift to lower values since austenite content will be lower. But there may not be a corresponding shift in curve 2, as the ferrite width will not be different. Hence, curve 1 will intersect curve 2 at lower values of fracture toughness and higher temperatures, as indeed shown in Figure 1.

But the experimental values are lower than the theoretically predicted values. One reason for this may be segre-

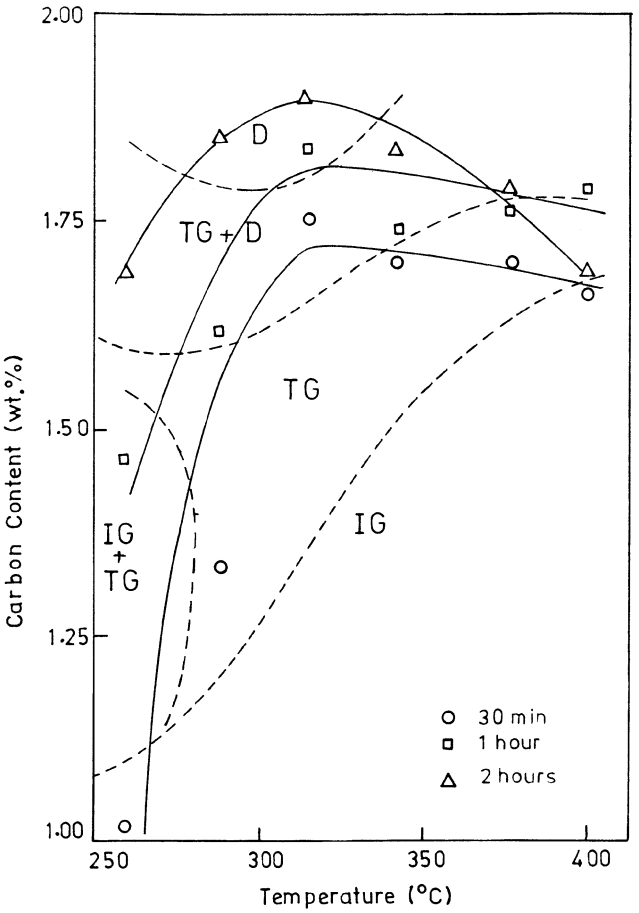

Fig. 11—Carbon content of retained austenite as a function of austempering temperature.

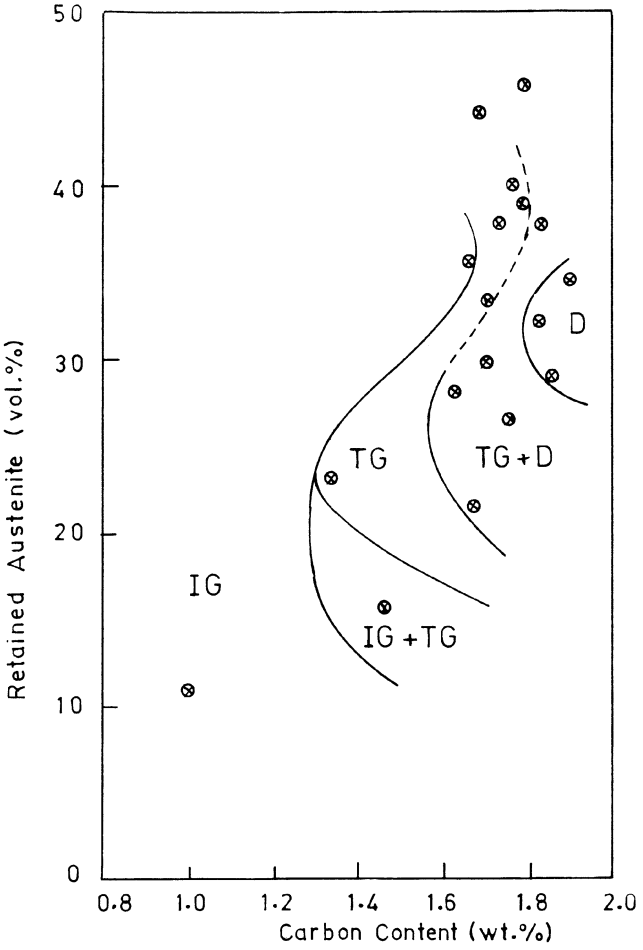

Fig. 12—Fracture mechanism at different austenite content and carbon content.

gation in the intercellular regions in the alloyed ADIs. These contain carbides and are also likely to contain martensite. These regions can have an adverse effect on the fracture behavior of the material, as shown by the results of Putatunda and Singh,[19] who have shown that unalloyed ADI has a higher fracture toughness than alloyed ADI.

As mentioned earlier, the first term inside the bracket in Eq. [8] is negligibly small. Therefore, according to Eq. [8], fracture toughness is proportional to the product $(X_\gamma^{1/2} \cdot n)$, showing that the strain hardening behavior of the austenite has an important influence on the fracture toughness. While strain hardening is basically due to dislocation–dislocation interactions, certain additional obstacles can enhance the work hardening. This may be due to strain-induced phase transformation, fine mechanical twinning, stacking fault–dislocation interactions, or dynamic strain aging. Several investigators[27,28,29] have attributed the rapid work hardening of high carbon austenites to the interaction of dislocations with carbon atoms in solid solution. It is interesting to note that rapid work hardening of a well-known high carbon austenite, *viz*. Hadfield manganese steel, is attributed to dynamic strain aging.[30] Adler *et al.*[31] too postulated that high carbon content of austenite plays a crucial role in its high work hardening through the formation of pseudotwins. It is therefore reasonable to expect that high strain hardening of austenite in ADI is due to the interaction between the dislocations and carbon atoms. This is further supported by the results of Shieh *et al.*,[32] who showed that dynamic strain aging occurs in ADI over a wide temperature range. Analysis of interaction between the misfit strain field of a carbon atom and the strain field of a dislocation gives an expression for solution hardening that is proportional to the square root of the solute concentration.[33,34,35]

We can therefore write

$$K_{Ic} \alpha (X_\gamma C_\gamma)^{1/2} \quad [17]$$

where C_γ is the carbon content of the retained austenite.

In Eq. [16], τ_i, G, and γ_s are constants. For a given critical crack length, therefore, K_{IC} varies as $L^{-1/2}$. Hayrynen *et al.*[36] have shown that the yield strength of ADI can be expressed in terms of $L^{-1/2}$ by the following equation:

$$\sigma_y = AL^{-1/2} + BX_\gamma + C \quad [18]$$

where L is the ferrite particle size; X_γ is the volume fraction of retained austenite; and A, B, and C are constants. The preceding relation has been found to be valid by Ali *et al.*[37] also. Both investigators have shown that ferrite particle size is the dominant factor, and therefore, yield strength is essentially proportional to $L^{-1/2}$. Noting the dependence of K_{IC} on $L^{-1/2}$, wecan write

$$K_{Ic} \alpha \sigma_y \quad [19]$$

Combining, Eqs. [17] and [19], we arrive at

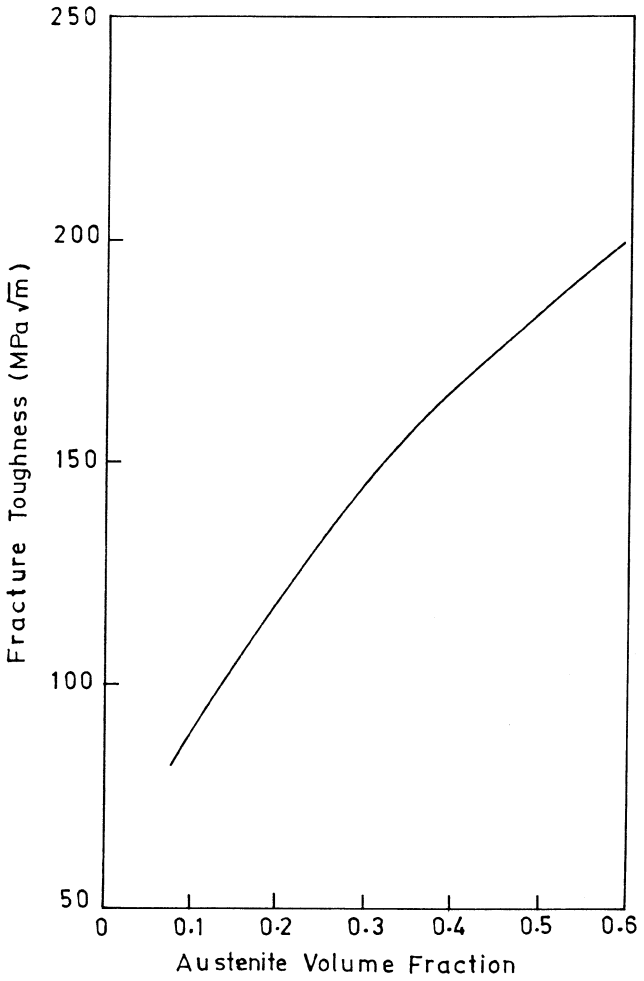

Fig. 13—Dependence of fracture toughness on volume fraction of retained austenite.

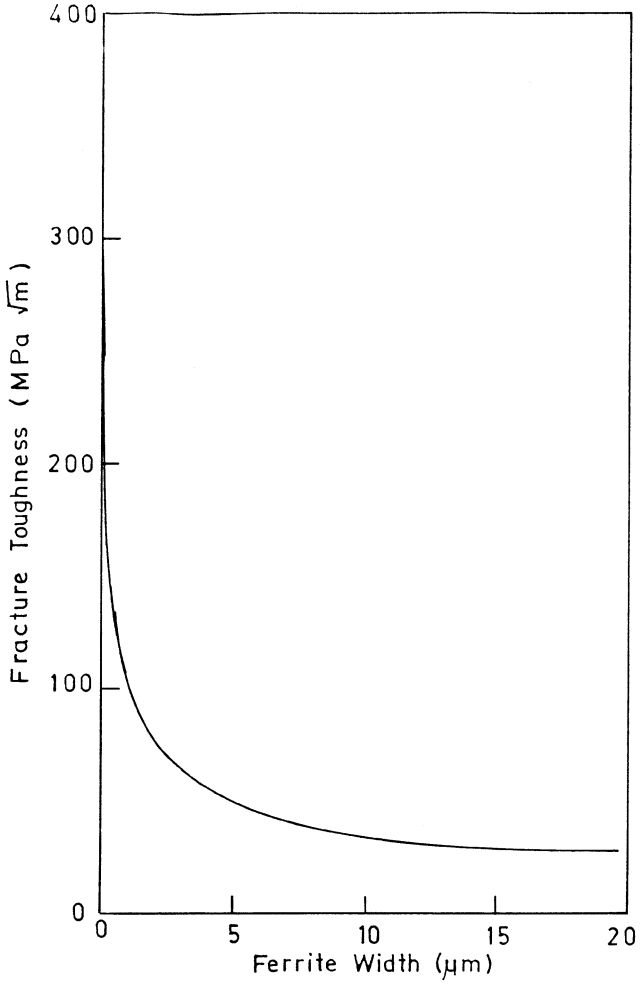

Fig. 14—Dependence of fracture toughness on width of ferrite blade.

$$K_{Ic}^2 \alpha \sigma_y (X_\gamma C_\gamma)^{1/2} \quad [20]$$

Therefore, according to the present model, a plot of K_{IC}^2 against the factor $\sigma_y (X_\gamma C_\gamma)^{1/2}$ must result in a straight line. This was verified using the X_γ and C_γ values reported in Figures 8 and 10. The yield strengths under different austempering conditions were estimated using Eq. [18]. Constants A, B, and C required for this were taken from the literature.[36] Ferrite particle size was estimated from the breadth of (211) diffraction peak of ferrite using the Scherrer formula:[38]

$$D = \frac{0.9\lambda}{\beta \cos \theta} \quad [21]$$

where D is particle size, λ is wavelength of radiation, β is peak width at half-maximum intensity, and θ is Bragg angle. The estimated values of yield strength are reported in Table II. These were used in plotting $\sigma_y (X_\gamma C_\gamma)^{1/2}$ against $(K_{IC})^2$ in Figure 16. Two points corresponding to samples austempered for 30 minutes and 1 hour at 260 °C were left out, as they exhibited intergranular fracture due to incomplete transformation. A straight line was drawn by the method of least squares. A correlation coefficient of 0.9 was obtained showing that Eq. [20] is obeyed reasonably well.

Table II. Yield Strengths after Various Heat Treatments as Estimated from Equation [18]

Austempering Temperature (°C)	Austempering Time		
	30 Minutes	1 Hour	2 Hours
	Yield Strength (MPa)		
260	1263	1184	1108
288	1127	1032	968
316	985	973	871
343	946	847	825
371	872	788	760
399	830	707	691

IV. CONCLUSIONS

1. Fracture toughness of ADI is dependent on austempering temperature. As the austempering temperature is increased, the fracture toughness initially increases, reaches a maximum at some intermediate temperature, and drops with further rise in temperature.
2. A model is developed to account for the variation of fracture toughness with austempering temperature. According to this model, the observed variation in fracture toughness with austempering temperature is due to the interplay between the effects of ferrite grain size and austenite volume fraction.

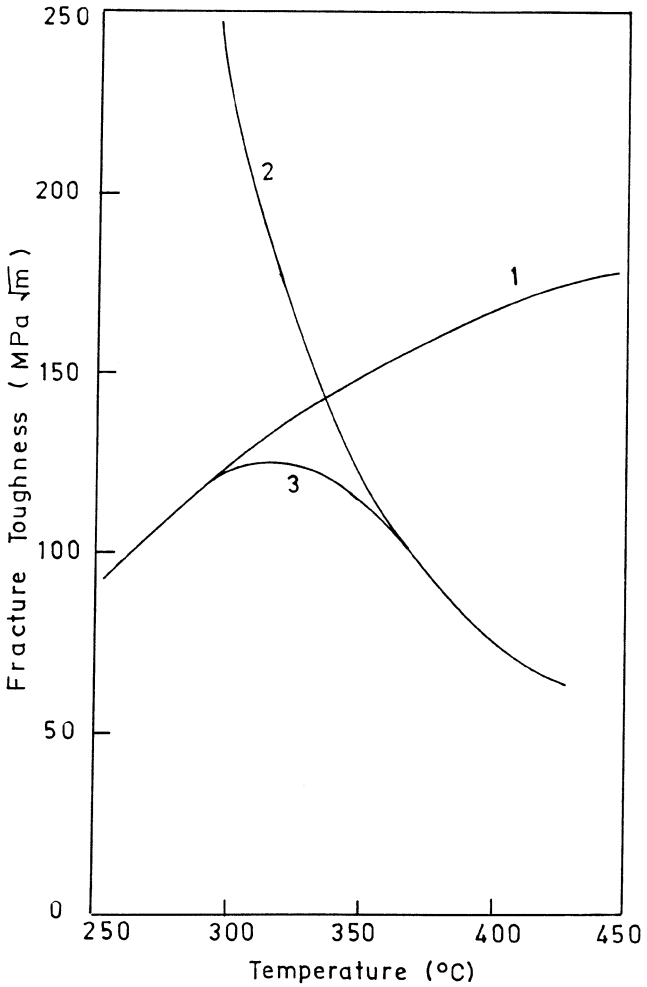

Fig. 15—Influence of austempering temperature on fracture toughness: 1—based on austenite content, 2—based on ferrite width, and 3—resultant curve.

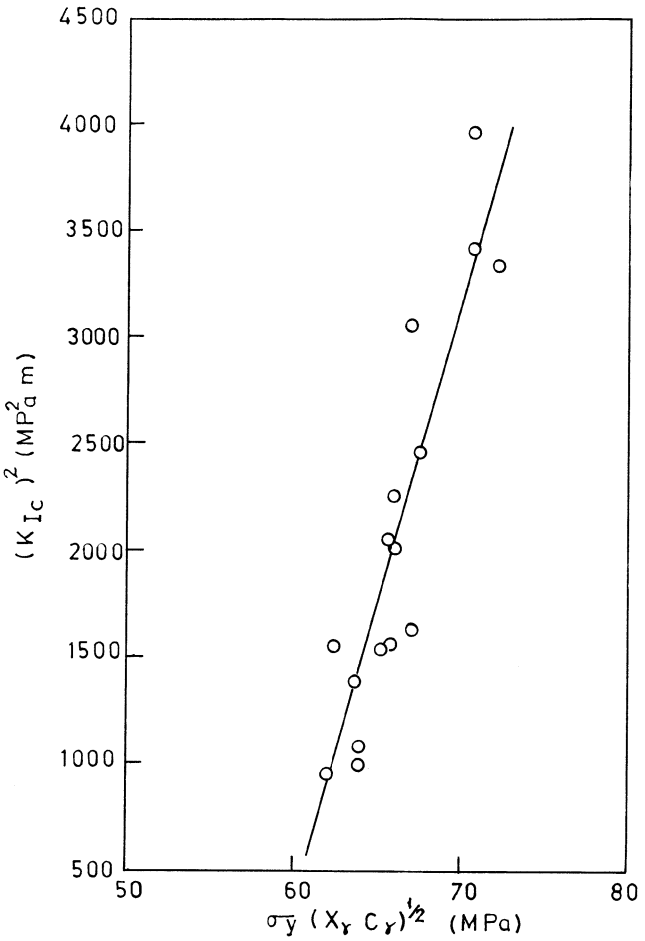

Fig. 16—Plot of K_{IC}^2 against $\alpha_y (X_{\gamma C\gamma})^{1/2}$

3. The model shows that the best fracture toughness is obtained when volume fraction of retained austenite is about 30 pct and carbon content of retained austenite is more than 1.8 wt pct. These conditions are satisfied when austempering is carried out in the temperature range of 300 °C to 320 °C.
4. A plot of K_{IC}^2 against $\sigma_y (X_{\gamma C\gamma})^{1/2}$ results in a straight line, as suggested by the model.

ACKNOWLEDGMENT

This work was financially supported by Ford Motor Company (Dearborn, MI).

REFERENCES

1. M. Johansson: *AFS Trans.*, 1977, vol. 85, pp. 117-22.
2. J. Dodd: *Hod. Cast.*, 1978, vol. 68 (5), pp. 60-66.
3. R.B. Gundlach and J.F. Janowak: *Met. Progr.*, 1985, vol. 128 (2), pp. 19-26.
4. R.A. Harding and G.N.J. Gilbert: *Br. Foundryman*, 1986, vol. 79, pp. 489-96.
5. K.B. Rundman and R.C. Klug: *AFS Trans.*, 1982, vol. 90, pp. 499-508.
6. J. Janowak and R.B. Gundlach: *AFS Trans.*, 1983, vol. 91, pp. 377-88.
7. T.N. Rouns, K.B. Rundman, and D.M. Moore: *AFS Trans.*, 1984, vol. 92, pp. 815-40.
8. D.J. Moore, T.N. Rouns, and K.B. Rundman: *AFS Trans.*, 1987, vol. 95, pp. 765-74.
9. N. Darwish and R. Elliott: *Mater. Sci. Technol.*, 1993, vol. 9, pp. 572-85.
10. N. Darwish and R. Elliott: *Mater. Sci. Technol.*, 1993, vol. 9, pp. 882-89.
11. J. Aranzabal, I. Gutierrez, J.M. Rodriguez-Ibabe, and J.J. Urcola: *Mater. Sci. Technol.*, 1992, vol. 8, pp. 263-73.
12. I. Bartosiewricz, I. Singh, F.A. Alberts, A.R. Krause, and S.K. Putatunda: *J. Mater. Eng. Perf.*, 1993, vol. 4, pp. 90-101.
13. S.K. Putatunda and I. Singh: *J. Test. Eval.*, 1995, vol. 23, pp. 325-32.
14. S.K. Putatunda, R. Gupta, and P.P. Rao: *Microstr. Sci.*, 1996, vol. 24, pp. 103-10.
15. P.P. Rao and S.K. Putatunda: *Metall. Mater. Trans. A*, 1997, vol. 28A, pp. 1457-70.
16. J.L. Doong, F.C. Ju, H.S. Chen, and L.W. Chen: *J. Mater. Sci. Lett.*, 1986, vol. 5, pp. 555-58.
17. J.L. Doong and C.S. Chen: *Fat. Fract. Eng. Mater. Struct.*, 1989, vol. 12, pp. 155-65.
18. R. Voigt, H. Dhame, and L. Eldoky: *Proc. 2nd Int. Conf. on Austempered Ductile Iron*, Ann Arbor, M1, 1985, Gear Research Institute, Naperville, IL, 1986, p. 327-40.
19. Z.K. Fan and R.E. Smallman: *Scripta Metall. Mater.*, 1994, vol. 31, pp. 137-41.
20. G.T. Hahn and A.R. Rosenfield: *Applications Related Phenomena in Titanium Alloys*, ASTM STP 432, ASTM, Philadelphia, PA, 1968, p. 5.
21. R. Honeycombe and H.K.D.H. Bhadeshia: *Steels—Microstructure and Properties*, Edward Arnold, London, 1995, p. 24.
22. G.E. Dieter: *Mechanical Metallurgy*, McGraw-Hill, New York, NY, 1986, p. 282.

23. L.E. Murr: *Interfacial Phenomena in Metals and Alloys*, Addison-Wesley, Reading, MA, 1975, p. 185.
24. B.P.J. Sandvik: *Metall. Trans. A*, 1982, vol. 13A, pp. 777-87.
25. L. Sidjanin and R.E. Smallman: *Mater. Sci. Technol.*, 1992, vol. 8., pp. 1095-2006.
26. L. Sidjanin, R.E. Smallman, and S.M. Boutorabi: *Mater. Sci. Technol.*, 1994, vol. 10, pp. 711-23.
27. W.N. Roberts: *Trans. TMS-AIME*, 1964, vol. 230, p. 373.
28. C.H. White and R.W.K. Honeycombe: *J. Iron Steel Inst.*, 1962, vol. 200, pp. 457-66.
29. G. Collette, C. Crussard, A. Kohn, J. Plateau, G. Pomey, and M. Weisz: *Rev. Metall.*, 1957, vol. 54, pp. 433-81.
30. Y.N. Dastur and W.C. Leslie: *Metall. Trans. A*, 1981, vol. 12A, pp. 749-59.
31. P.H. Adler, G.B. Olson, and W.S. Owen: *Metall. Trans. A*, 1986, vol. 17A, pp. 1725-37.
32. C.S. Shieh, T.S. Lui, and L.H. Chen: *Mater. Trans. JIM*, 1995, vol. 36, pp. 620-37.
33. P.M. Kelly: *J. Aust. Inst. Met.*, 1971, vol. 16, pp. 104-18.
34. M.Z. Butt and P. Feltham: *J. Mater. Sci.*, 1993, vol. 28, pp. 2557-578.
35. D. Peckner: *The Strengthening of Metals*, Reinhold, New York, NY, 1964.
36. K.L. Hayrynen, D.J. Moore, and K.B. Rundman: *AFS Trans.*, 1990, vol. 98, pp. 471-80.
37. A.S.H. Ali, K.I. Uzlov, N. Darwish, and R. Elliott: *Mater. Sci. Technol.*, 1994, vol. 10, pp. 35-45.
38. B.D. Cullity: *Elements of X-ray Diffraction*, Addison-Wesley, Reading, MA, 1978, p. 102.